Heriot-Watt University, Institute of Petroleum Engineering

University of Edinburgh, Grant Institute of Earth Sciences

University of Newcastle, School of Civil Engineering and Geoscience

Supervisor - Rachel Wood

MSc GeoSEAD

Project Report 2010/2011

João Soares de Albergaria Cabral Barata

Cementation dynamics in a Middle Eastern carbonate reservoir

Declaration:

I, João Soares de Albergaria Cabral Barata, confirm that this work submitted for assessment is my own and is expressed in my own words. Any uses made within it of the works or other authors in any form (e.g. ideas, equations, figures, text, tables, programs) are properly acknowledged at the point of their use. A list of the references employed is included.

Signed:

Date:

1 Acknowledgements

I wish to express my gratitude to my supervisor, Dr. Rachel Wood, whose guidance and support helped me achieve an understanding of the subject.

I would like to thank PhD student, Dean Thorpe, for all his support; Dr. Adrian Finch of the University of St. Andrews for making the cathodoluminescene microscope available and Dr. John Craven for all the technical support in the Ion Microprobe facility.

Lastly, I am grateful to ADCO (Abu Dhabi Company for Onshore Oil Operations) for providing and giving the permission to use information on the area assessed in this study.

2 Summary

The present diagenetic study targets a reservoir formation from the Lower Cretaceous Thamama Group, which was deposited in an Abu Dhabi intrashelf basin within the bigger Rub Al Khali basin of the south Arabian gulf. It contains important carbonate oil fields defined by gentle anticlinal structures, producing around 5 % of the world oil.

The aim of this study is to give a better understanding of the cementation dynamics in a Lower Cretaceous Middle East carbonate reservoir of the Thamama Group by assessing the controls on reservoir quality and the effects of oil charge. This was performed using data from two wells; one in crest position and the other in a flank position by analyzing the differences in volumetric evolution of diagenetic cements between coeval oil and water leg samples.

This was achieved using cathodoluminescence methods to identify cement growth and zonation, isotopic analysis (ion microprobe) and microscopic analysis using UV light to detect oil inclusions and to identify the relative timing of oil and water leg cement creation.

Syntaxial calcite cement overgrowths in the oil leg are divided into five main zones based on the cathodoluminescence colour zonation, showing ion microprobe $\delta^{18}O$ values between -3.03 in the earlier cements and -11.57 in the latest, allowing for a cement stratigraphy to be defined. The ferroan cement in the water leg occludes pore space in totality and shows $\delta^{18}O$ values between -4.61 and -8.20, with no obvious cement stratigraphy.

Oil inclusions were identified in early syntaxial cement zones, with $\delta^{18}O$ values of approximately -5. This was identified as the earliest oil charge event, allowing to compare the volume of cement in the oil and water leg following the start of oil emplacement, which causes the major changes in diagenetic evolution to the reservoir rock in crest position.

Oil charge retards diagenesis in the oil leg, with 77 to 85 % less cement precipitating when compared to the water leg during this same diagenetic stage.

3 Table of Contents

4 Objective

The aim of this study is to give a better understanding of the cementation dynamics in a Lower Cretaceous Middle East carbonate reservoir of the Thamama Group by assessing the controls on reservoir quality and the effects of oil charge. It focuses on petrographic methods and the analysis of burial cement volumes in coeval oil and water leg samples, based on $\delta^{18}O$ trends obtained through cathodoluminescence (CL) and ion microprobe methods.

Oil charge lowers water saturation to a minimum level, known as the irreducible water saturation, bringing the diagenetic processes to a halt. This will retard or avoid further cementation, preserving porosity and permeability. In the water leg, fluid flow continues through the pore network as a whole, maintaining a high rate of cementation occluding most of the pore space.

Based on the cathodoluminescence colour zonation and oxygen isotope data, cement volumes will be calculated in samples from both legs, with the expectation to find different diagenetic behaviours, with different cement growth rates, hence showing different cement volumes as a consequence of oil emplacement in the crestal area.

With further work, the timing of the cement formation and the diagenetic environment in which they were formed can be obtained, helping in the understanding of the evolution of pore-filling fluids and diagenetic processes through time as well as in developing and improving burial models.

This will help in the development of carbonate basin and reservoir models and in the improvement of exploration and field development plans in carbonates, enabling better oil reserves estimates and an increase in production potential.

5 Background

5.1 Geological setting

The Arabian peninsula has an approximate area of 3x106 Km^2. It is bounded to the West and South by the Red Sea rift and Gulf of Aden rift, respectively, to the North by the thrust zones of the Alpine Orogeny and to the East by the orogenies of the Zagros thrust belt and the Oman mountains (Figure 2). The major morphological units in the peninsula are, from West to East, the Arabian-Nubian Shield, the interior shelf (interior homocline), the outer shelf and the orogenic margins of the block, observed in the Omani and Zagros mountain ranges (Henson, 1951, and Powers et al., 1966).

The geological formation, known as the Thamama Group, analyzed in this study was deposited in the areas adjacent to the Abu Dhabi intrashelf basin, in the Rub Al Khali basin (Figure 2), which was created within the Arabian platform in the southern Arabian gulf, during the Aptian (Alsharhan, 1995).

5.2 Tectonic evolution

During the Palaeozoic (latest proterozoic and early Cambrian, Beydoun, 1991), consolidation and accretion of the Arabo-Nubian shield to the Gondwana margin went through, with clastic sediments being deposited in the surrounding shallow epeiric seas of the Middle Eastern area and no major tectonic activity being recorded (latest proterozoic to late paleozoic, Beydoun, 1991).

The ancient Arabian shield is presently seen in the Western part of the peninsula and dips towards the East, forming the basement of the interior shelf and of the outer unstable shelf.

In the late Permian, the beginning of extensional and rifting events caused the drifting away of the central Iran, northwest Iran and part of Turkey blocks from the Gondwanan margin, leading to the opening of the Neotethys sea.

The rifting of the Gulf of Aden and the Red Sea during the Eocene represents the breaking of Gondwana, the separation of the Arabian plate from Africa and its collision with Asia, creating the major tectonic events presently observed in the northeastern margins of the Arabian plate (Beydoun, 1991):

The collision of the Arabian and Eurasian plates formed the Zagros fold belt, with the subduction of the Arabian platform under the Eurasian plate leading to the surface placement of ophiolites in Oman ending in the Eocene. These rifting events together with the Alpine Orogeny in the Miocene/Pliocene, bring the Rub Al Khali basin, where the Thamama Group is located, to its present form (Alsharhan et al., 2001).

The regional anticlinal structure affecting the Thamama Group was created by two major stages; an East-West folding and closure followed by a North-South closure. The structure has a length of 35 km and a width of 10 km (Oswald, 1995). The structural changes in the area started in the Cenomanian, with no major events being found during the time of deposition of the Thamama (Oswald, 1995).

During the Cenomanian, the surface placement of ophiolites in the Eastern area of the Arabian platfrom created the East-West antiform closure and folding, causing the reactivation of the horst and graben basement structures. This reactivation displaced the overlying sediments, creating several anticlinal and synclinal changes in the substrata of the southern area of Abu Dhabi (Oswald, 1995).

In the Campanian, a North-South anticlinal structure started forming with a more ponounced southward dip of the strata, leading to the creation of East-West faults (perpendicular to the tilting) in the existing East-West anticline. During the late Tertiary, the last structural event goes through, with the northward tilting of the northern limb coinciding with the tectonic events related to the Zagros mountain range creation, which is believed to have caused the lithosphere to bend to the north (Oswald, 1995).

The Hormuz salt deposited during the Infracambrian was also a cause for several structural changes starting in the Jurassic in this region, causing the displacement of overlying units, forming anticlinal structures and creating various producing oil fields in the area (Alsharhan et al., 2001).

The Thamama Group of the lower Cretaceous in Abu Dhabi, U.A.E., was deformed in this way, where gentle anticlinal structures were created and where important oil fields are producing around 5% of the world oil from the reservoirs of the Thamama Group, assessed in the present study. Several fold trends and antiform axis are shown in Figure 3, with the oil fields represented in green.

5.3 Stratigraphy

Clastic sedimentation was dominant in the area until the late Permian when there was a change to carbonate dominated sedimentation (Alsharhan, 1997). Stable shelf conditions were created, typifying the Jurassic as well as the Cretaceous when shallow-water carbonates accumulated on the shelf and inner Arabian platform, alternating with units of sabkha-like interbedded evaporites in the Jurassic (Beydoun, 1991). Between the Permian and the Jurassic, the carbonate shelf is exposed to dry sub-aerial conditions, with evaporitic basins forming in the area (Alsharhan et al., 2001).

The beginning of the Cretaceous marks the end of this evaporitic depositional phase and the return to a carbonate marine shelf depositional system controlled by marine transgressive cycles (Schlumberger, 1981).

The Thamama group was created in the Lower Cretaceous, and is affected by the regional anticlinal structure mentioned in section 5.2. It refers to the interval located between the top Tithonian and base Albian, ending with a regional unconformity surface (Figure 4), and has a layer cake stratigraphy with the reservoir zones being interlayered with argillaceous limestones (Figure 5) acting as seals between the major reservoir rocks of the group (Alsharhan et al., 2001).

The group contains the major reservoirs in Abu Dhabi with carbonate sediments originating from open shelf to shallow water depositional environments. It is divided into the four major reservoir formations Habshan, Lekhwair, Kharaib and Shuaiba.

The Lekhwair and Kharaib are characterized by cyclicity between open marine packstones and argillaceous mudstones spread throughout an extended area, representing the cyclicity in relative sea level change. The thicker dense limestone units together with the reservoir unit form a shoaling upward sequence, as shown in Figure 4. The open shelf environment represented in these two formations changes into an intrashelf basin depositional environment in the Shuaiba formation of the upper Thamama.

The sealing argillaceous limestone originated in transgressive phases, with sedimentation happening in deeper sea waters while the clean limestone, where the hydrocarbon accumulation are found, represent the regressive stage of a cyclic pattern (Figure 5) (Schlumberger, 1981).

The most important reservoir rocks in the UAE are found in rudist and algae rich carbonate deposited in the shallow waters of the Aptian, where many Abu Dhabi giant fields are in production (Alsharhan et al., 2001).

5.4 Petroleum system

Most of the hydrocarbon producing reservoirs in the Arabian peninsula are found in the Mesozoic, with particular reference to the reservoir units of the Thamama group mentioned in this study.

These contain the biggest volume of oil found in the area around Abu Dhabi, specifically in the zones A, B and C of the Thamama Group, with high reservoir rock porosity and moderate to low permeability. The oil found in these zones has an API gravity between 37 and 40^{o}. (Schlumberger, 1981)

The source rocks for the hydrocarbons trapped in the Thamama reservoirs are believed to be found in the Upper Jurassic Dukhan-Diyab, with migration beginning in the Late Cretaceous and being dominated by vertical pathways in places where the evaporitic seals in between are thin or absent. These source rocks are confirmed to be regionally extensive and to have reached sufficient levels of maturity to provide the volumes of hydrocarbon found in the Mesozoic and, specifically, the Early Cretaceous Thamama group reservoir rocks (Beydoun, 1991).

The Thamama A, B and C reservoirs are vertically separated by dense sealing carbonate layers (Figure 5), with the trapping mechanism being enhanced by the previously mentioned extensive and gentle anticline structure (Beydoun, 1991).

5.5 Diagenesis

The diagenetic study of carbonate rocks is of high importance as they help understanding the variation of rock properties and spatial heterogeneity in the exploration and development of carbonate reservoirs.

Reservoir quality is changed by diagenetic processes in the way they greatly affect and alter porosity, rock permeability and fluid flow through the rock. These processes are mainly controlled by the mineralogy of the matrix, the chemical composition and flow rate of the pore water and also physical factors such as compaction.

Cementation occurs as part of these diagenetic processes, when the fluid flowing through pore space is saturated in respect to the mineral phase found in the matrix grains. The chemical elements in high concentration find optimum nucleation sites on the surface of existing grains with similar chemical composition, causing different types of overgrowths and cementation processes which reduce pore space. Part of the cementation occurs during early diagenesis, as unstable Aragonite and High-Mg calcite dissolve and precipitate as low-Mg calcite, which is more stable and less soluble. With further diagenetic transformations, low-Mg calcite can also convert into the more stable carbonate mineral Dolomite. Cementation continues with burial until stability is reached in the chemical reactions between fluid and grain portions of the system.

Relative changes in sea level control the weathering conditions the sediment is exposed to and lead to different types of diagenetic processes, characteristic of each diagenetic realm. There are three different major diagenetic realms the sediment can be exposed to where different cementation processes lead to different cement fabrics: the meteoric, marine and burial realm.

The sediments in the meteoric vadose zone contain a mixture of water and air in the pore space. Precipitation distribution is irregular, leading to the formation of gravitational pendant and meniscus cements (sometimes showing in the marine vadose zone). In the meteoric phreatic zone, with higher water content and very little or no air, isopachous crusts and cement rims start forming on the grains surface consisting of equidimensional calcite crystals (Figure 6).

In the marine realm, where pore space is completely fluid-filled, drusy, equant and granular mosaic textures form, as well as syntaxial echinoderm overgrowths (Figure 6). With deep burial and increase in pressure and temperature, stylollites form perpendicular to the principal force direction, as a response to pressure dissolution.

The assessment of the different types of cements is of high interest to understand the diagenetic evolution of the sediments, identify the different realms and pore fluids they were exposed to and period of time they were exposed to each.

Petrographic analysis using optical and cathodoluminescence methods, together with geochemical analysis of fluid inclusions and isotopes in the cement overgrowths help achieve the final objective of understanding the diagenetic evolution of the rock and the impact of these processes on reservoir quality.

5.6 Oil leg vs water leg

Hydrocarbon charge lowers water saturation to a minimum level, known as the irreducible water saturation, bringing the diagenetic processes to a halt. This will retard or avoid porosity and permeability reduction, with macropores being preserved and maintaining a higher reservoir quality than the sediment in the water leg. The smaller pore spaces retain volumes of water within the oil leg and, assuming a water-wet rock, diagenesis continues, even if at significantly lower rates than in the water leg. If the rock is oil-wet, the grains will be covered by a thin hydrocarbon sheet reducing interaction between grain and fluid phase, avoiding further cementation.

In the water leg, fluid flow continues through the pore network as a whole, maintaining a high rate of cementation where the fluid is saturated in respect to the cement phase and occluding most of the pore space.

6 Data summary

The present study was based on thin sections of plug samples drilled from cored wells from the oil and water leg of the same reservoir unit, with the difference in burial depth between oil and water leg samples being approximately 210 m.

Three cement overgrowths were targeted for ion microprobe analysis; two from one thin section in the oil leg and one from a thin section in the water leg.

The small number of samples analyzed could be non-representative of the reservoir unit but are useful to give an understanding on the differences in diagenetic cement volumes between both legs.

7 Methods used

7.1 Petrographic analysis

A petrographic microscope was used to identify the sedimentary facies and the evolution of the diagenetic processes affecting the reservoir rock. Four thin sections from coeval surfaces were analyzed for this purpose; two from the oil leg and two from the water leg.

The diagenetic history was assessed by determining the relative timing of diagenetic events based on the relation between different cement phases visually observed.

The sedimentary facies were identified using the Dunham classification scheme, based on the depositional texture, the nature of the grains, and content in biogenetic material.

7.2 Cathodoluminescence

A cathodoluminescence Cold cathode CITL 8200 MK3A was used to find syntaxial overgrowths with distinguishable cement zonation, build thin section maps and identify targets for sampling in the ion microprobe.

Syntaxial cements growing from echinoderm fragments show zonation when observed under the cathodoluminescence microscope, presenting an identifiable cement stratigraphy. The luminescent response of these cement zones is controlled by the presence of the trace elements Mn2+ and and Fe2+, stimulating and reducing luminescence, respectively.

7.3 Porosity analysis

Full images of two thin sections, one from the oil leg and the other from the water leg, were produced using between 60 and 70 individual photos captured using the cathodoluminescence microscope with an attached digital camera (Figure 13). Using an image editing software, pore space was identified through thresholding processes creating a series of different binary images in order to obtain a range of values for porosity (Figure 7).The average value was taken as an indicator for the rock porosity in the area.

7.4 Oil Inclusions

Oil inclusions were located using a Leitz Metallux Leica 3 microscope with a 100 W Hg HBO 103 W/ 2 bulb and a blue filter creating UV light with a waveband of 440 to 490 nm. The inclusions identified were assessed as primary as they contained a portion of vapor phase. The cement phase where the oil inclusions were found will provide information on the relative timing of oil charge.

7.5 Isotopic analysis

Cement zones were targeted for sampling in a Cameca 1270 ion microprobe with special attention given to syntaxial overgrowths as they contain early cement phases, growing from echinoderm fragments, on to late cement phases growing into the pore space, allowing for a complete sequence of the cement stratigraphy to be analyzed. The cathodoluminescence

cement zonation allowed us to determine directions of sampling in order to obtain transects of $\delta^{18}O$ data, from early to late cement phases, independently of the colour zonation.

The samples were gold-coated and a Cs ion beam was used to remove 10 to 15 µm diameter samples from the thin section. The external precision was calculated as 0.2 ‰, determined from analysis of a University of Wisconsin calcite standard considered as being homogeneous.

Two syntaxial overgrowths were targeted on one thin section from the oil leg and two other targets were identified in one thin section from the water leg, both thin sections being from a coeval surface. Six transects were completed following the defined targets on the syntaxial cements.

7.6 Volumetrics

Based on the cathodoluminescence colour zonation, areas for the different syntaxial cement phases were calculated as a proxy for the respective volumes. The cement areas of the two ion microprobe targets were calculated using CL images and an image editing software and are assumed to represent the cement growth areas in the assessed formation.

Another 20 targets identified on samples from a different reservoir unit in the same area were also calculated, as they were found in higher quantity, in order identify any visible trends related to cement growth.

The volume of the porosity occluding ferroan cement, which is the major cement phase in the water leg samples was also calculated and compared to the volume of cement with similar ^{18}O values in the oil leg. ^{18}O data give an indication of temperature and depth, suggesting similar ^{18}O values would correspond to a similar diagenetic stage.

At the same diagenetic stage, cement growth is expected to be different in the oil leg and water leg as a consequence of oil charge, hence showing different cement volumes.

8 Results and Discussion

8.1 Facies

Bioclastic skeletal and algal components observed in the thin sections are green algae, echinoderm fragments, orbitolinids, benthic foraminifers, gastropod fragments and a small amount of bivalve fragments.

Analyzing the depositional texture, the rock shows relatively high mud content and also high content of bioclasts and peloids (Figure 21). Although contact between grains is observed, the rock is considered to be originally mud supported and undergone post-depositional compaction, reducing pore space and increasing grain contact during burial.

Following the Dunham classification scheme the reservoir rock in this area can be described as Algal, Skeletal, Peloid Wackestone to Packstone.

Based on this classification and the identification of orbitolinids in the thin sections observed (Figure 21), the sediments were interpreted as being deposited in a middle carbonate ramp depositional environment, according to the model presented by ADCO, 2004 (Figure 9).

8.2 Diagenesis

For samples from the water leg, the following diagenetic processes were identified and summarized in Figure 10:

- Early cementation leading to calcite precipitation on grains' surface created a calcite rim and an early phase of porosity reduction.

- Aragonite dissolution in skeletal remains and fragments, promoted by undersaturation of the pore fluid relative to the grains, leads to the creation of moldic porosity.

- The dissolved material is then transported to precipitate elsewhere in a later cementation phase. This cementation occurs as blocky, intergranular calcite, reducing porosity and permeability and enhancing rock stifness. Cementation first starts on optimum nucleation sites like echinoderm fragments where syntaxial cements grow.

- Dolomitization occurs as recrystallization and replacement of calcite crystals as isolated dolomite rhombs are observed in the last cement phase.

- Compaction and pressure solution goes through with increasing burial when higher temperature and pressure conditions promote the fracturing of grains and cement crystals and the creation of stylollites (Figure 21). This leads to further dissolution and intergranular cementation, reducing macroporosity and increasing the contribution of microporosity to the reservoir development.

Syntaxial cements and late ferroan cements show different fracture orientation, suggesting the sediment was exposed to different force fields developed through time in this location.

The cement phases occlude most of the primary porosity, leaving secondary porosity as the major network for fluid flow through the reservoir, suggesting an increasingly important role of microporosity in the rock behavior.

The observed cement fabrics and evolution during diagenesis suggests the sediment was exposed to a marine phreatic diagenetic realm, followed by shallow and deep burial diagenetic realms.

The oil leg, however, shows a different diagenetic evolution, with oil emplacement retarding diagenesis. The last cement phase in the water leg, occluding the intergranular pore

space, is not found in the oil leg, meaning oil charge happened somewhere in between the earlier cementation phases.

From the oil inclusion analysis, evidence is found for oil emplacement during a relatively early diagenetic stage. Oil inclusions with a vapour bubble, which indicates it is a primary inclusion, were found in an early dark brown cement zone of a syntaxial overgrowth (Figure 11). Comparing to the targets sampled in the ion microprobe, this zone would correlate with an area within zones 2 and 3, with $\delta^{18}O$ values between -4 ‰ and -7 ‰.

8.3 Porosity

The average porosity of the oil leg sample obtained for the different threshold values applied during the image analysis was 21,3 % (Table 1), while the result of a petrophysical analysis using helium injection on samples from a single well at approximately the same depth was 30 %, with an average value of 24,8 % for the reservoir formation (ADCO study, 2004). If compared to the average value of 24,8 % for the reservoir rock, 21,3 % is a relatively good approximation.

Table 1. Porosity calculated from cathodoluminescene photo, after thresholding (**Figure 7**).

Threshold limits	Total area (pixels)	Pore area (pixels)	Porosity (%)
115-255	3281867	399017	12.1
120-255	3281867	496906	15.1
123-255	3281867	580620	17.6
125-255	3281867	649126	19.7
127-255	3281867	742674	22.6
130-255	3281867	867535	26.4
135-255	3281867	1164249	35.4
		Average	**21.3**

The difference between the values obtained using the two different methods; image analysis and helium injection; is due to the microporosity of the samples. From microscopic observation, it is noticed that microporosity is the most abundant type of porosity in the analyzed sample. The epoxy resin in the thin section is stained blue, hence, showing the pore space in blue (Figure 12). Microporosity is said to comprise between 51 and 90 % of total porosity (ADCO study, 2004).

There is uncertainty regarding the values obtained when using the image analysis method as the thin section is not representative of the whole volume and the production of the binary image leads to errors in interpretation due to the ambiguity regarding the similar colour of cement phases and pore space in the cathodoluminescence photos used when thresholding.

In the water leg, due to continuation of cementation after oil charge brings cementation to a halt in the oil leg, the image analysis method is not useful in calculating the porosity of the sample. Calcite cementation is extremely high below the oil-water contact in the flank position when compared to the crest position, with the last cement phase occluding great part of the macroporosity. The difficulty increases when trying to identify pore space during image analysis of water leg samples as microporosity gives the main contribution for total porosity. Pore space is distinctly identified as black colour in the oil leg image as opposed to the water leg image where the darker colour represents the ferroan cement phase (Figure 13). When creating the binary image, there is no distinct colour representing porosity, in order to define acceptable thresolding levels. Results from laboratory petrophysical analysis using helium injection show a porosity of 15,7 % in the water leg (ADCO, 2004).

The image analysis observations show there is a porosity reduction from the crest zone to the flank position. This is supported by laboratory tests that show a decrease in porosity from 24,8 % in crest position to 11,5 % and 15,7 % in flank positions. (ADCO, 2004).

Furthermore, the same study shows that the average pore diameter reduces from 0,69 µm in crest position to 0,47 µm in flank position (ADCO, 2004).

8.4 $\delta^{18}O$ Analysis

Figure 15 and Figure 16 show the isotopic data collected form a syntaxial cement overgrowth from the oil leg and how the same colour zone may contain a range of $\delta^{18}O$ values. In Figure 15, the light blue zone ranges from -3.37 ‰, on the left side of the grain, to -4.60 ‰ on the right side of the grain.

Samples were collected along four transects, with data summarized in Table 2. The direction of the transects is shown in Figure 17. Transect 3 has been divided into transects 3.1 and 3.2 as growth directions are sampled twice, with the cement growing to the centre of the pore space.

The different cathodoluminescence zonation represents the pore water variation in Mn^{2+} and Fe^{2+} content while the values for $\delta^{18}O$ in the water vary with temperature and burial and are not linked with the colors shown by the luminescence. In other words, the same type of pore water may precipitate and create cement with similar luminescence characteristics but show changing $\delta^{18}O$ values as burial depth increases.

The syntaxial cements targeted in the oil leg samples show five different zones based on the colour zonation and ion microprobe data (Table 2 and Figure 17), with $\delta^{18}O$ values ranging from -3.03 ‰ and -3.37 ‰ in early cements to -9.61 ‰ and -11.37 ‰ in later cement zones. The two targets in the oil leg show the same zonation configuration and correlation between isotopic data, showing similar trends (Figure 18).

Table 2. $\delta^{18}O$ values along the transects shown in Figure 17.

	Transect 1 (T1)	Transect 2 (T2)	Transect 3 (T3)	Transect 4 (T4)
Zone 1				
Zone 2	-3.37	-4.17 -4.55 -4.6		
Zone 3	-6.02	-5.38	-7.02 -6.97	-6.75 -6.37
Zone 4	-9.17 -9.61	-8.81		-9.3 **-9.4**
Zone 5			-11.51 -11.31 -11.32 -11.37 -11.25	-11.27 -11.86 -11.05
Zone 4			-8.16	
Zone 3			-6.9 -6.99 -5.43	
Zone 2				
Zone 1			-3.03	

T3.1

T3.2

The high difficulty level in identifying points of reference in the thin section from the water leg caused the data to be sampled in a different location than the target previously defined. The isotopic data from the water leg was sampled from the latest pore-filling ferroan cement phase; which is non-existent in the oil leg as consequence of early hydrocarbon charge; instead of the intended syntaxial overgrowths. $\delta^{18}O$ values of this late ferroan cement range from -4.61 ‰ to -8.20 ‰ (Figure 14). This suggests that the major pore spaces would have been filled by this cement phase during the period of early syntaxial cementation observed in the oil leg samples.

This is in agreement with the oil inclusion observations mentioned in Section 8.2 and confirms the diagenetic processes would have slowed down at around this time in the crest position. Oil inclusions were found in a cement zone where $\delta^{18}O$ data shows a value of approximately -5 ‰. This value is linked to a certain depth and temperature and, hence, to a

certain diagenetic stage. While in the flank positions cementation continued at a high rate after this stage, with the ferroan cement occluding the pore space in totality, in the crest zone cementation was retarded and cementation occurred with much lower volumes.

8.5 Volumetrics

The volumetric analysis on the syntaxial cements of the 20 targets is summarized in Table 6.

Data was sorted in an ascending order of pore space to show cement growth trends related to pore space availability. The pore space was measured as the immediate empty space surrounding the grain before cementation occurs. Compaction is not taken into account as there was no available method to quantify it, which adds to the uncertainties of the method.

As would be expected, the syntaxial cement zones get bigger with greater available space to grow (Figure 19). What should be noticed is that each zone fills a percentage of the empty pore space and that there is very little variation in this percentage with the variation in pore size (Figure 20). This can be explained as the area of the pore section influences the fluid flow through the pore space (Darcy Law) which, in turn, influences the rate and amount of material transported and, as a consequence, the rate of cementation on nucleation sites.

These results were obtained from a different reservoir formation in the area, where a higher quantity of syntaxial overgrowths was found, to help understand how cement grows in the subsurface as part of the diagenetic process.

Petrographic analysis of the thin sections from the formation that is being assessed in this study shows the pore filling ferroan cement is not present in the oil leg, while in the water leg it represents the major part of cementation. Oil emplacement in the crest area reduces

available pore space for water flow and retards cementation, preventing this ferroan cement to grow and occlude pore space.

In the water leg, the ferroan cement starts growing at a diagenetic stage where the oxygen isotpe analysis shows a maximum value of -4.61 ‰ and decreases to a minimum value of -8.20 ‰ as burial depth and temperature increase. For this cement growth not to be present in the oil leg would mean oil emplacement should happen at a burial depth where isotopic analysis shows similar values to the earliest ferroan cement phase in the water leg, which would be around -5.

Oil inclusions in the oil leg were found in a cement zone where $\delta^{18}O$ data shows a value between -4 ‰ and -7 ‰. This means the earliest oil charge in the reservoir rock at the crest zone could have started at around -4 ‰ or -5 ‰; which is in accordance to the cementation processes observed in the water leg, where the ferroan cement strarts growing at approximately the same time.

The volume of cement growing in the water leg was compared to the volume of cement growing in the oil leg during the same time, in order to show the different cementation rates and the effect that oil emplacement has in the diagenetic process. Cement zones showing isotopic values between -4.61 ‰ and -8.20 ‰ would have been created in the same depth interval, with the same temperature conditions. This corresponds to the total amount of ferroan cement in the water leg and to zones 2 and 3 of the syntaxial overgrowths in the oil leg.

A binary image for the thin section from the water leg was created to calculate the volume of ferroan cement, with the cement phase being represented by the darker colours. A series of binary images was created with different threshold values applied, from which an average value was obtained (Figure 8 and Table 3). As this cement phase occludes the pore space, the percentage of cement in the rock will be the same as the initial porosity.

Table 3. Cement volume calculated from cathodoluminescene photo, after thresholding.

Threshold limits	Total area (pixels)	Ferroan cement area (pixels)	Cement percentage (%)
115-255	3281867	750208	22.9
120-255	3281867	803644	24.5
123-255	3281867	840703	25.6
125-255	3281867	868180	26.5
127-255	3281867	898449	27.4
130-255	3281867	949102	28.9
135-255	3281867	1050421	32
		Average	**26.8**

To compare the volume of cement in the oil and water leg, the syntaxial overgrowth ion microprobe targets (Figure 15 and Figure 16) were used. The volume of cement zones 2 and 3, corresponding to the same diagenetic stages as the ferroan cement zone, was calculated and compared to the volume of the inital pore space in the same target zone, after backstripping the syntaxial overgrowths. The initial pore space is assumed to correspond to the ferroan cement volume that would have grown in this target zone, according to observations of the water leg thin section where it is seen to be pore occluding. The results are summarized in Table 4 where the relation between the two cements is shown. The immediate observation is that during the same diagenetic stage, 77 to 85 % less cement precipitates in the oil leg. This difference is a consequence of fluid flow reduction caused by oil emplacement.

Table 4. Relation between ferroan cement and syntaxial cement of the same diagenetic stage. Areas, as proxies for volumes, are measured in pixels.

	Initial pore space (predicted ferroan cement)	Zone 2+3	Zone 2+3 / Ferroan cement
Target 1	31567	4572	0.15
Target 2	23918	5546	0.23

The different rate of cement growth in the oil and water leg after oil charge in the crest zone is expressed by the gradients of the functions shown in Figure 1, with the ferroan cement growing to occupy up to seven times more volume than the corresponding syntaxial cement.

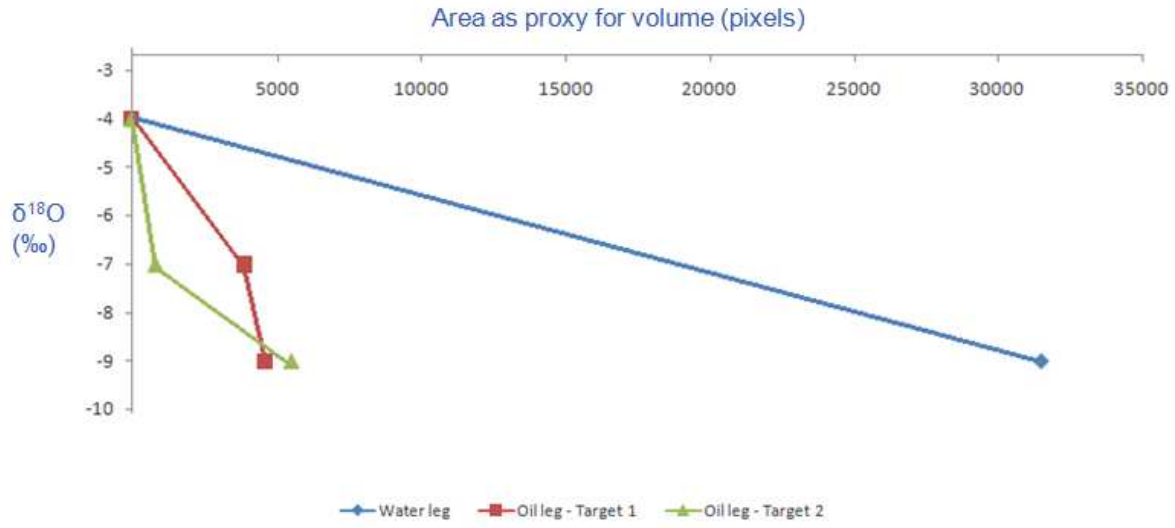

Figure 1. Cement volume growth with decrease in $\delta^{18}O$.

While the ferroan cement in the water leg grows to completely occlude pore space, in the oil leg, syntaxial cements grow to occupy 54 to 57 % of the initial pore space immediately surrounding the grain (Table 5).

Table 5. Volume of syntaxial overgrowths as percentage of initial pore space.

	Initial pore space (pixels)	Syntaxial Cement (pixels)	Syntaxial Cement / Initial pore space
Target 1	31567	17189	0.54
Target 2	23918	13742	0.57

9 Uncertainties

Uncertainty levels regarding the methods used in this study are high as the cement volumes were calculated for two individual grains and pore spaces immediately surrounding them. They do not represent the full thin section and the method cannot be extended to the whole thin section area as the targeted cements are not found in all pore spaces.

The results obtained give us an understanding of the different growth rates of the oil and water leg cement phases during the same diagenetic stages. To obtain results that represent cement growth volumes in the full reservoir rock in the area, an extension of the method to the whole thin section must be accomplished with δ18O analysis of different cement targets, as well as extending the observations and analysis to different thin sections, in order to cover a bigger volume of the reservoir rock.

The methods used were applied to 2D images which adds to the uncertainties. An extension of the methods to a 3D analysis via Pore Architecture Methods (PAMs) would help reduce the uncertainty levels and achieve more accurate results. PAMs provide for better results when assessing porosity and pore networks by analyzing a cubic sample of the reservoir rock built from 3 thin sections cut orthogonally from the plug sample.

The image editing processes and interpretations also add to the uncertainty levels. The definition of cement zones is limited by the quality of the thin section, as we can only analyze a 2D section of the 3D cement overgrowth.

The area of the 2D cross-section of the cement overgrowth observed on the thin section is used as a proxy for the volume calculation. This will add to the uncertainties as, depending on the point the thin section is cut from, the cement overgrowth cross-sections show different areas and high variability between them.

10 Conclusions

The present diagenetic study was performed using data from two wells; one in a crest position and the other in a flank position by analyzing the volumetric evolution of diagenetic cements in the oil and water legs.

From thin section petrographic analysis the rock was classified as Algal, Skeletal, Peloid Wackestone to Packstone. Based on the defined macrofacies and on the presence of orbitolinids, the rock was identified as having been originated in a middle carbonate ramp depositional environment, according to the model presented by ADCO, 2004.

Oil inclusion analysis shows the first oil charge evidence at an initial stage of the syntaxial overgrowths in the oil leg which corresponds to the early ferroan cement in the water leg. This ferroan cement phase is non-existent in the oil leg, which proves the idea that oil emplacement alters cementation dynamics.

Ferroan cement in the water leg is the major cement phase and grows to occlude macroporosity, recording $\delta^{18}O$ values between -4.61 ‰ and -8.20 ‰. By comparing the $\delta^{18}O$ values of this cement phase in the water leg to the syntaxial overgrowths in the oil leg, it is possible to define the syntaxial zones that grew during the same diagenetic stage, in order to compare cement growth and its response to oil emplacement.

Oil charge brings water saturation levels to an irreducible level, decreasing water flow through the pore network and decreasing the amount of transported material available to precipitate. This leads to a smaller rate of cement growth when compared to the growth rate in the water leg.

Volumetric analysis of the oil and water leg cement zones created during the same diagenetic stage (same depth interval) shows that the ferroan cement in the water leg grows to occupy seven times more volume than the syntaxial cements in the oil leg, with the syntaxial

cement zones in the crest position growing to approximately 15 % of the total ferroan cement. This is supported by petrophysical data, which shows a porosity reduction from 24 % in the oil leg to 15 % in the water leg.

Burial cementation seems to be the main control on reservoir quality, destroying it in the water leg, while oil emplacement preserves it in the oil leg. Only in certain places cementation is found to occupy up to 57 % of a single pore.

This analysis confirms that oil charge retards cementation, preserving porosity and permeability, and provides an understanding of the cement growth dynamics.

11 Suggestions for further work

To further complement this study, a larger number of cement overgrowth targets from a variety of different wells in the area should be analyzed to help validate and improve the quantification methods used.

A 3D analysis of thin section images using PAMs (Pore Architecture Models) can be done to improve the prediction of petrophysical properties of the reservoir rock.

Temperature and depth profiles should be used to build a relationship between $\delta^{18}O$ data and burial depth, in order to improve the understanding of rock response to water flow and cementation dynamics, linking it to the environmental and structural evolution of the area.

A carbonate reservoir model can then be built, including cementation effects and relating them to porosity and permeability evolution.

12 References

Alsharhan, A.S., Nairn, A.E.M., 2003. Sedimentary basins and petroleum geology of the middle east. Elsevier, Amsterdam.

Alsharhan, A.S., Rizk, Z.A., Nairn, A.E.M., Bakhit, D.W., Alhajari, S.A., 2001. Hydrogeology of an arid region: The Arabian Gulf and adjoining areas, Chapter 3. Elsevier, Amsterdam.

Beydoun, Z.R., 1991. Arabian plate hydrocarbon geology and potential - A plate tectonic approach. AAPG Studies in Geology #33.

Bjorlykke, K., 2010. Petroleum Geoscience: From sedimentary environments to rock physics, Chapter 5. Springer, Berlin.

Cox, P.A., Wood, R.A., Dickson, J.A.D., Al Rougha, H.B., Shebl, H., Corbett, P.W.M., 2010. Dynamics of cementation in response to oil charge: Evidence from a Cretaceous carbonate field, U.A.E.. Sedimentary Geology 228, 246-254.

Flugel, E., 2010. Microfacies of carbonate rocks - Analysis, interpretation and application. Springer, Berlin.

Granier, B., Al Suwaidi, A.S., Busnardo, R., Aziz, S.K., Schroeder, R., 2003. New insight on the stratigraphy of the Upper Thamama in offshore Abu Dhabi (U.A.E.). Notebook on Geology, Article 2003/05.

Granier, B., 2000. Lower Cretaceous stratigraphy of Abu Dhabi and the United Arab Emirates - A reappraisal. The 9th Abu Dhabi International Petroleum Exhibition & Conference, Conference Proceedings, Abu Dhabi: ADIPEC, 0918, pp. 526-535.

Grotsch, J., Al Jelani, O., Al Mehari, Y., 1998. Integrated study of a faulted and fractured reservoir. http://brcgranier.pagesperso-orange.fr/gmeop/Esg2001/adipec_1998/Lyon-01.htm (last assessed on 2nd August).

Matos, J.E., 2011. Applied carbonate sedimentology course.

Murris, R.J., 1980. Middle East: Stratigraphic evolution and oil habitat. American Association of Petroleum Geologists Bulletin, v. 64, No. 5 (May 1980), p. 597-618.

Nichols, G., 2009. Sedimentology and stratigraphy, Chapters 15 and 16. Willey-Blackwell

Oswald, E.J., Mueller, H.W., Goff, D.F., Al Habshi, H., Al Matroushi, S., 1995. Controls on porosity evolution in Thamama Group carbonate reservoirs in Abu Dhabi, U.A.E.. SPE, 029797.

Sarg, R, <year>. Carbonate Diagenesis I - Diagenetic processes, environments, & products.

Schlumberger, 1981. Well evaluation conference, United Arab Emirates, Qatar. Schlumberger Middle East, Abu Dhabi.

Scholle, P.A., Ulmer-Scholle, D.S., 2003. A color guide to the petrography of carbonate rocks: Grains, textures, porosity, diagenesis. AAPG Memoir 77, 2003.

University College London, 2002. Microfossil image recovery and circulation for learning and education. http://www.ucl.ac.uk/GeolSci/micropal/welcome.html (last assessed on 2nd August).

Masse, P., Walgenwitz, F., Maza, C., 2004. UAE, ASAB Field, Diagenetic study and porous network characterization. Abu Dhabi Company for Onshore Oil Operations (ADCO), 2004. (Confidential Report).

13 Appendices

13.1 List of Tables and Figures

13.1.1 Tables

13.1.2 Figures

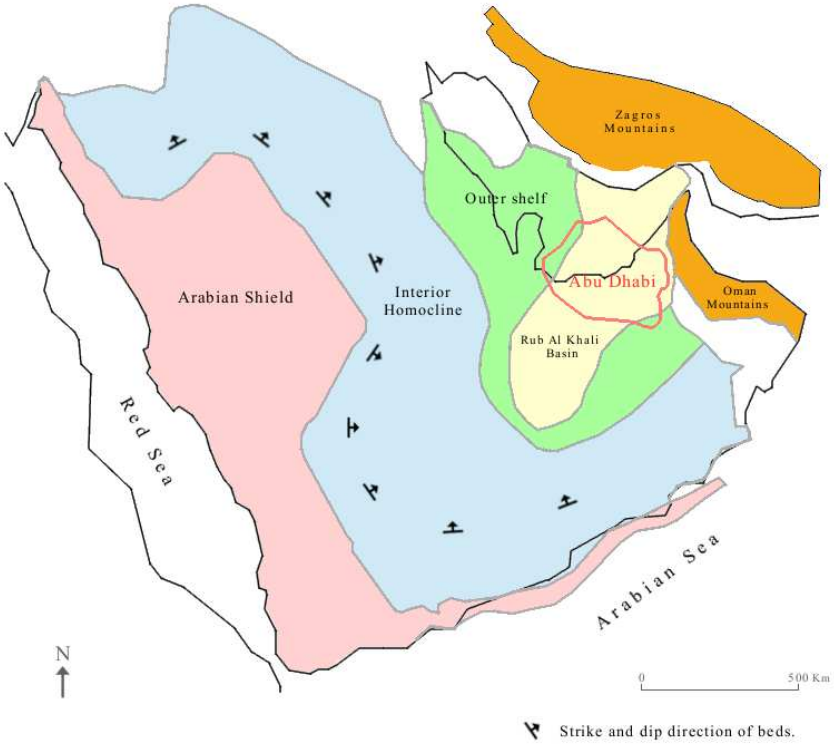

Figure 2. Main structural provinces of the Arabian Peninsula (modified from Schlumberger, 1981).

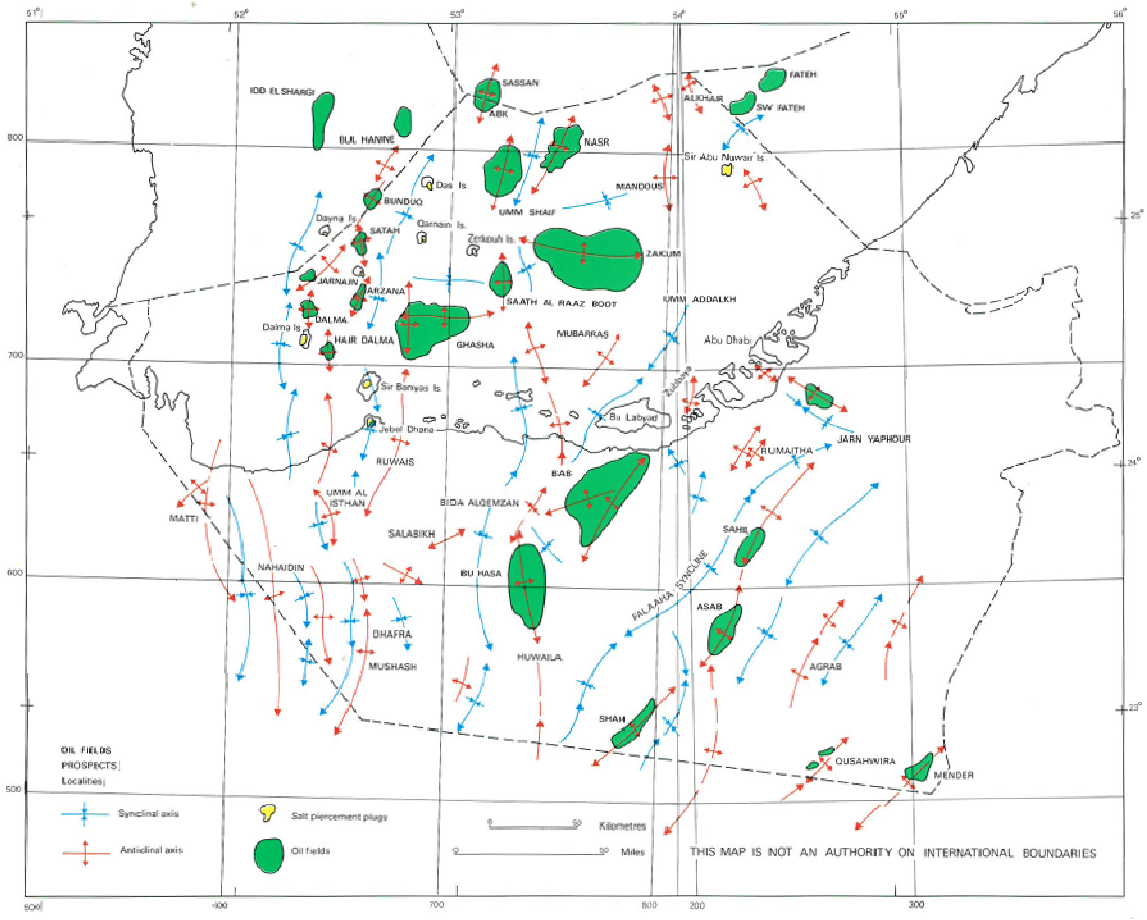

Figure 3. Main structural trends of the Arabian Peninsula (Schlumberger, 1981).

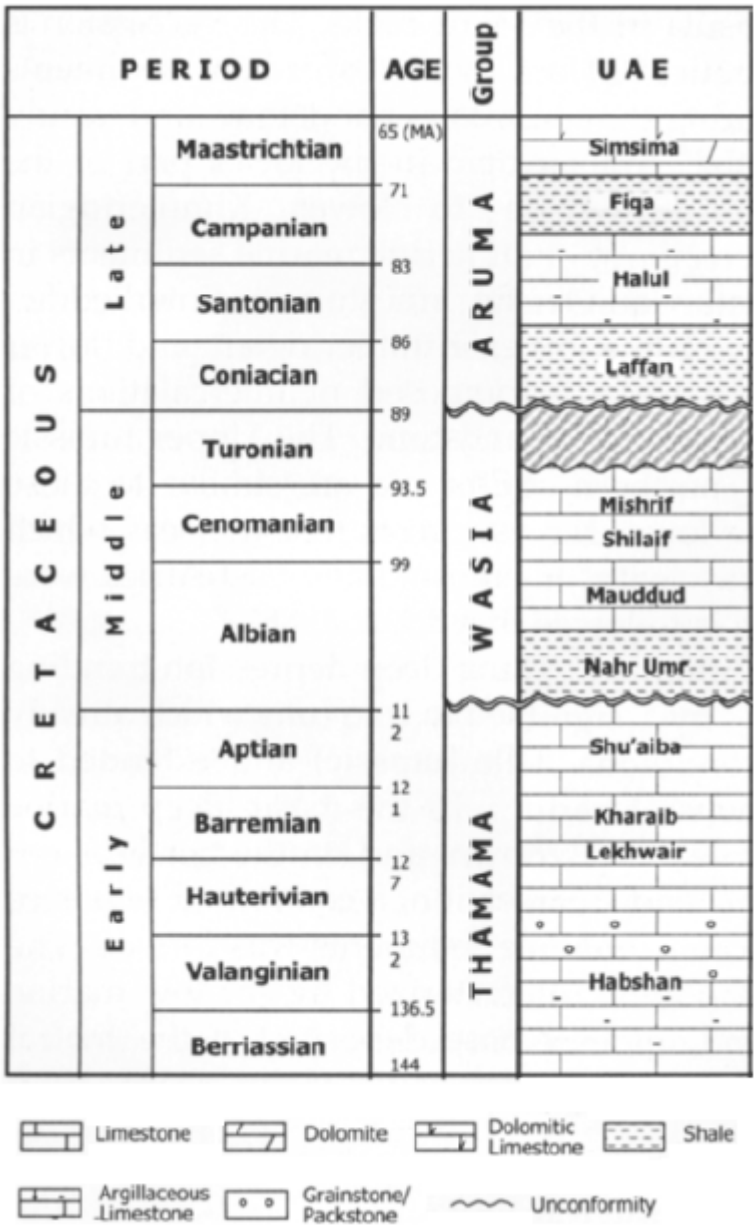

Figure 4. Stratigraphic column of the UAE (modified from Alsharhan, 2001).

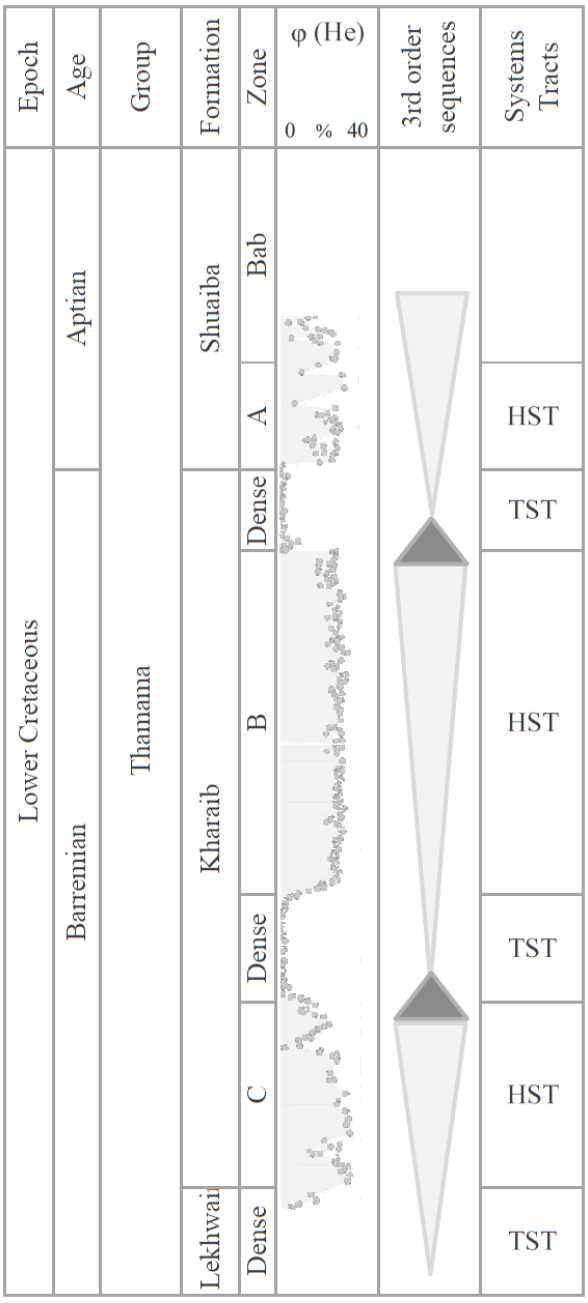

Figure 5 Sequence stratigraphic column. Based on data from ADCO, 2004 (modified from Alsharhan, 2003 and ADCO, 2004).

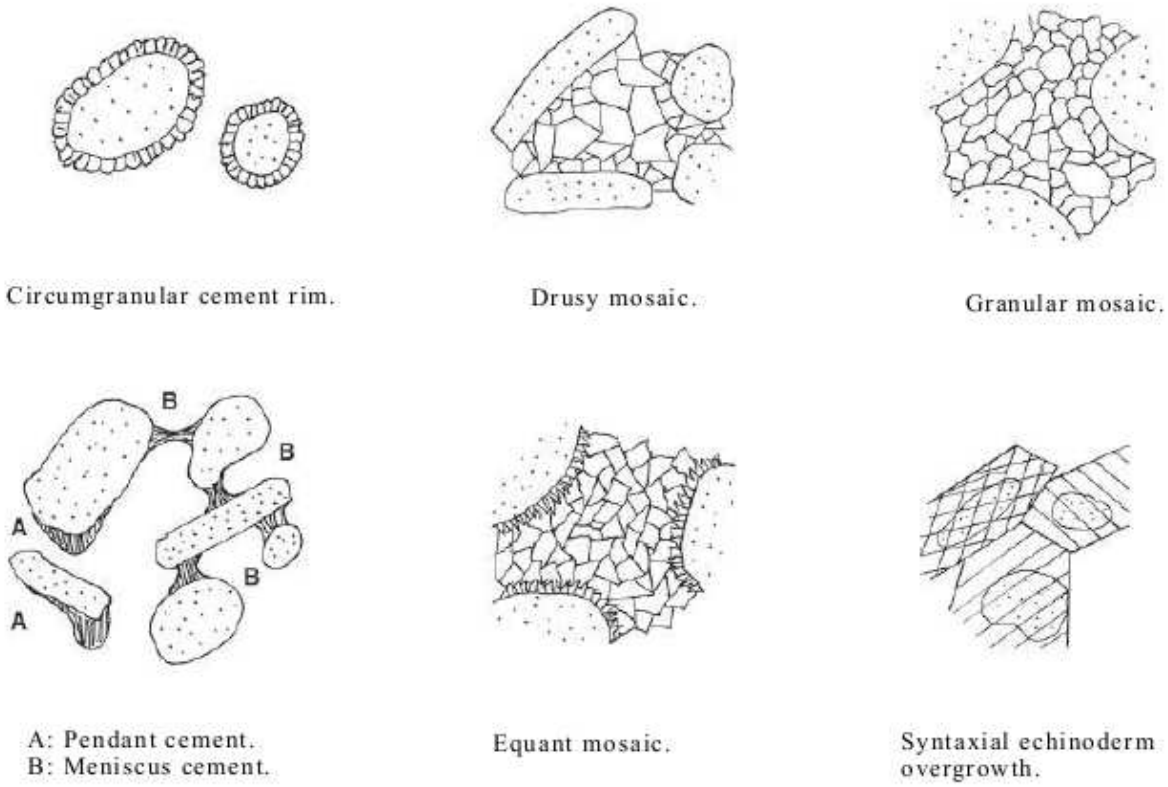

Figure 6: Cement fabrics (modified from Flugel, 2010).

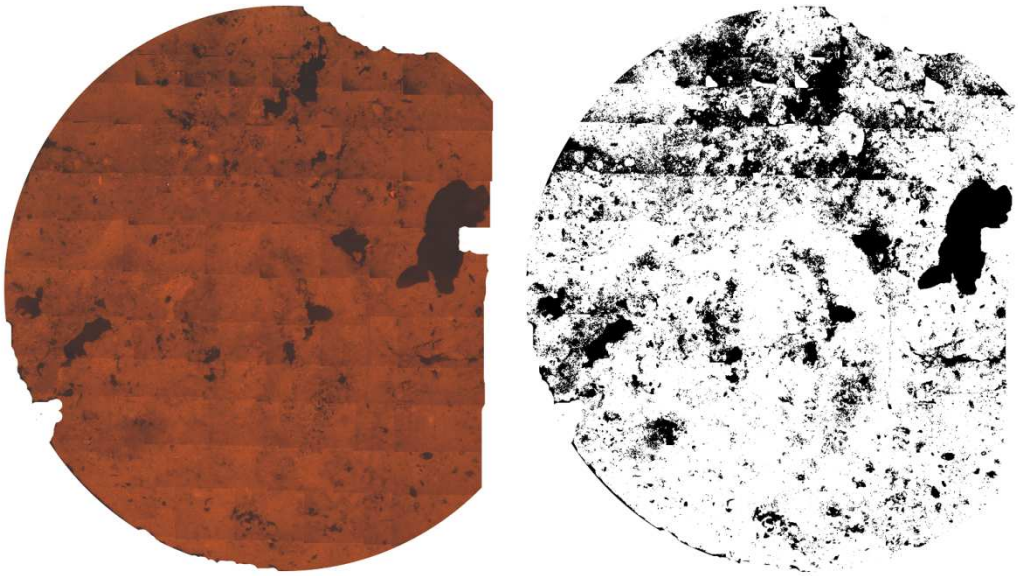

Figure 7. Left: Cathodoluminescence photo of the oil leg sample. Right: Binary photo after thresholding.

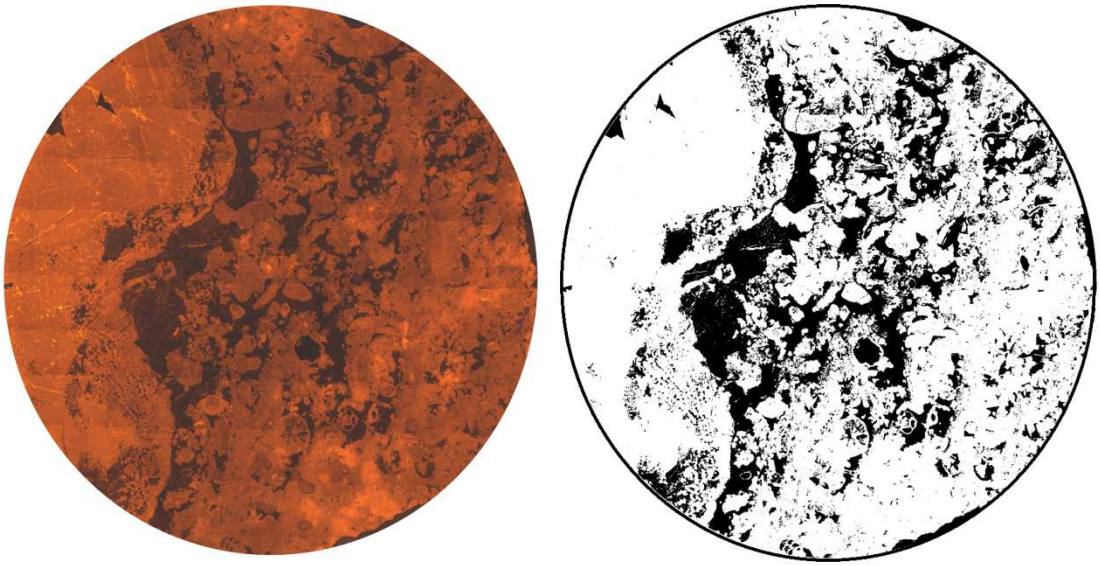

Figure 8. Left: Cathodoluminescence photo of the water leg sample. Right: Binary photo after thresholding.

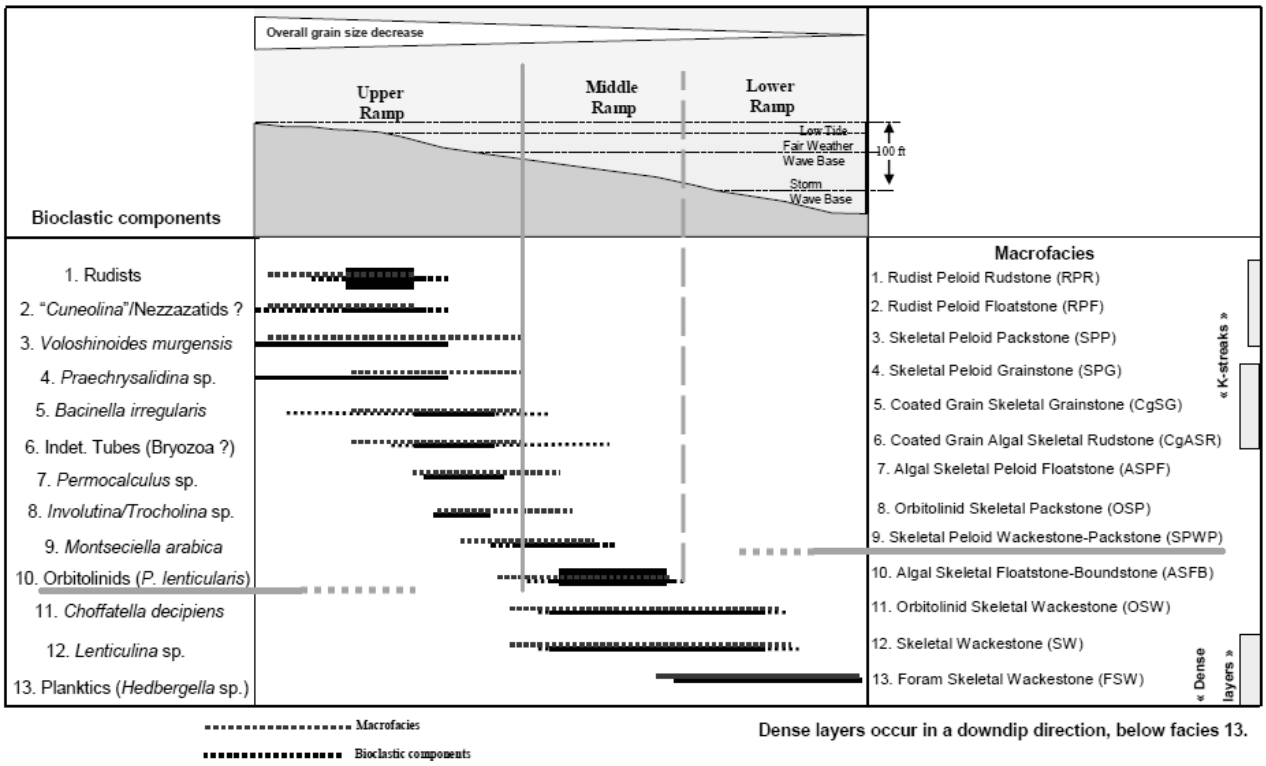

Figure 9. Depositional environment model showing the classification of the analyzed samples and their positioning in the model (modified from ADCO, 2004).

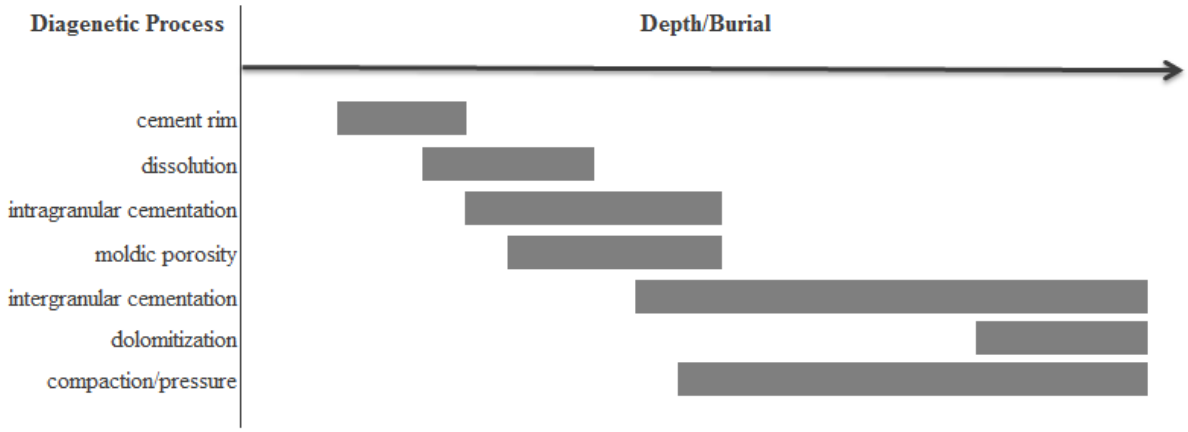

Figure 10. Diagenetic evolution as interpreted from petrographic analysis.

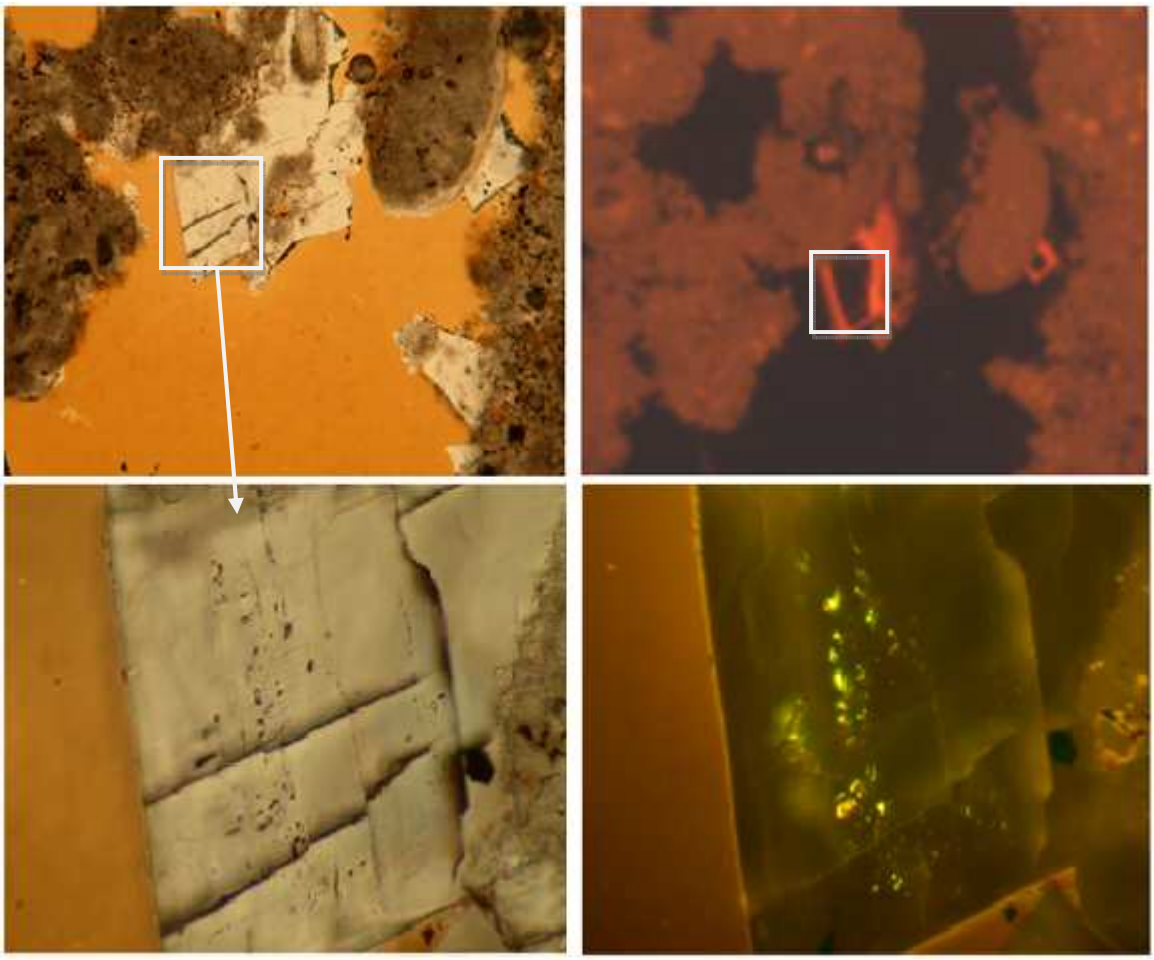

Figure 11. Top left: thin section under polarized light. Top right: Cathodoluminescense photo of same target. Bottom left: Oil inclusions under polarized light. Bottom right: Oil inclusions under UV light.

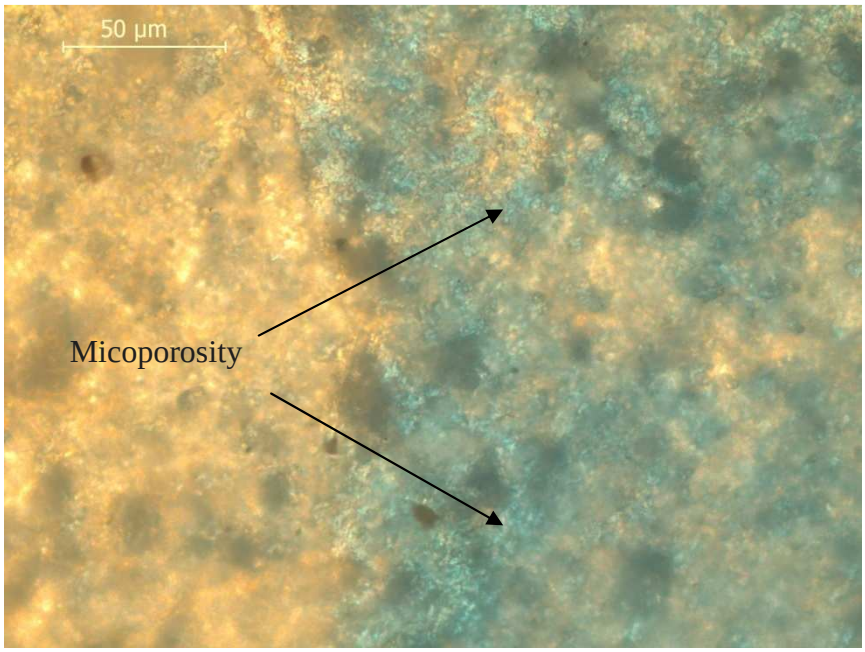

Figure 12. Oil leg thin section photo showing microporosity in blue.

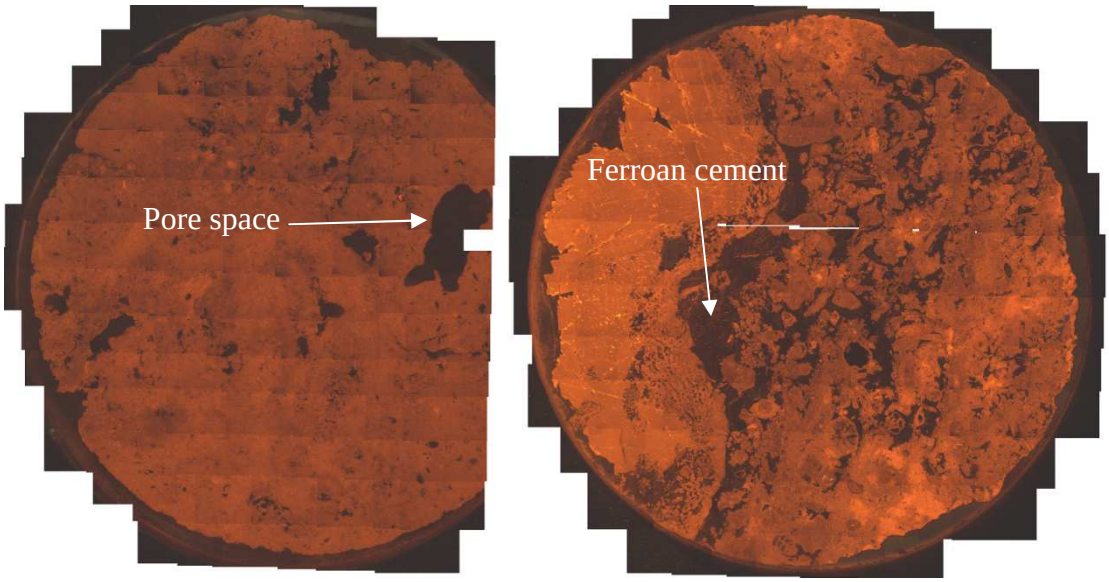

Figure 13. Cathodoluminescence photos showing pore space in dark colours (left) and ferroan cement, also in dark colours (right). Left: Oil leg. Right: Water leg

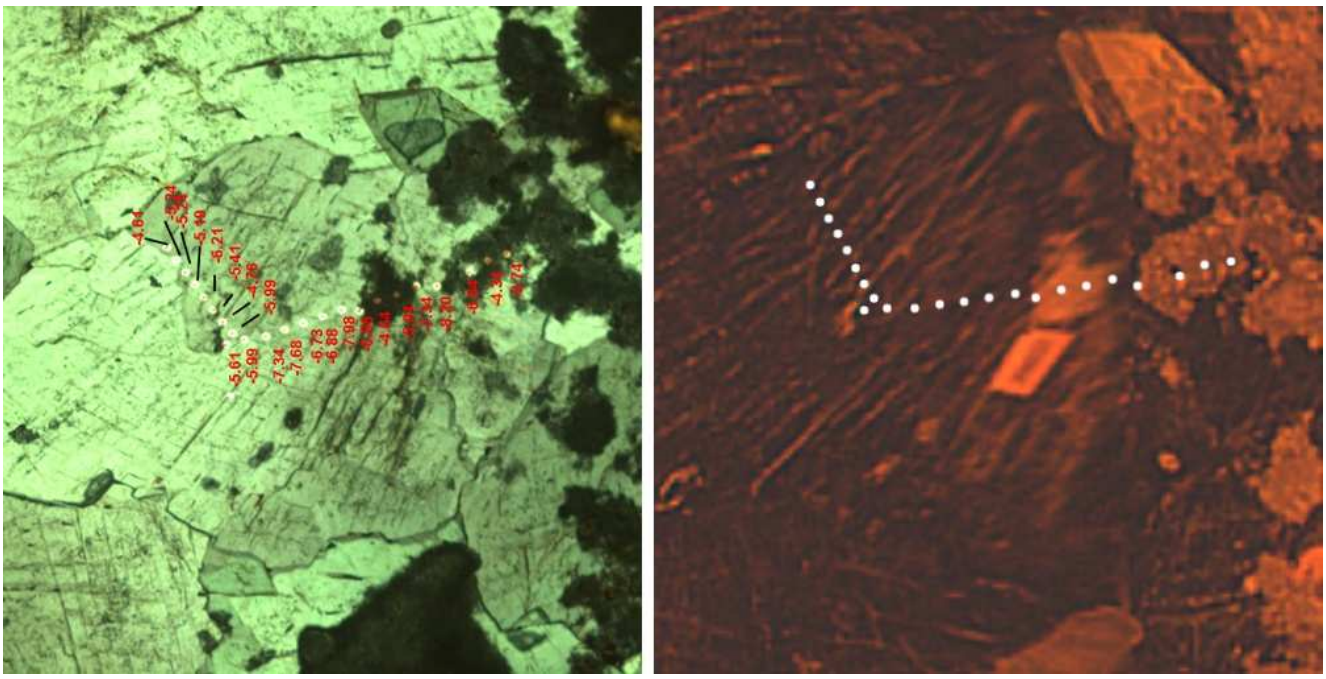

Figure 14. Water leg Ion Microprobe target showing $\delta^{18}O$ values. Cathodoluminescence image on the right.

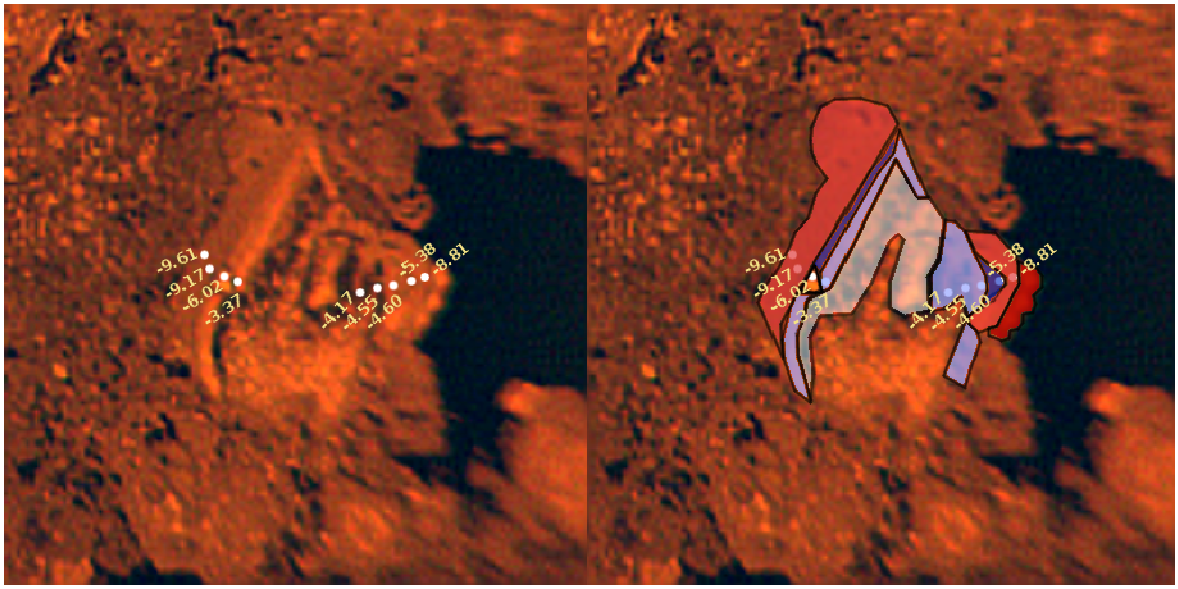

Figure 15. Cathodoluminescence photos of target 1 (oil leg) showing cement zonation (right) and oxygen isotope values decreasing away from the grain.

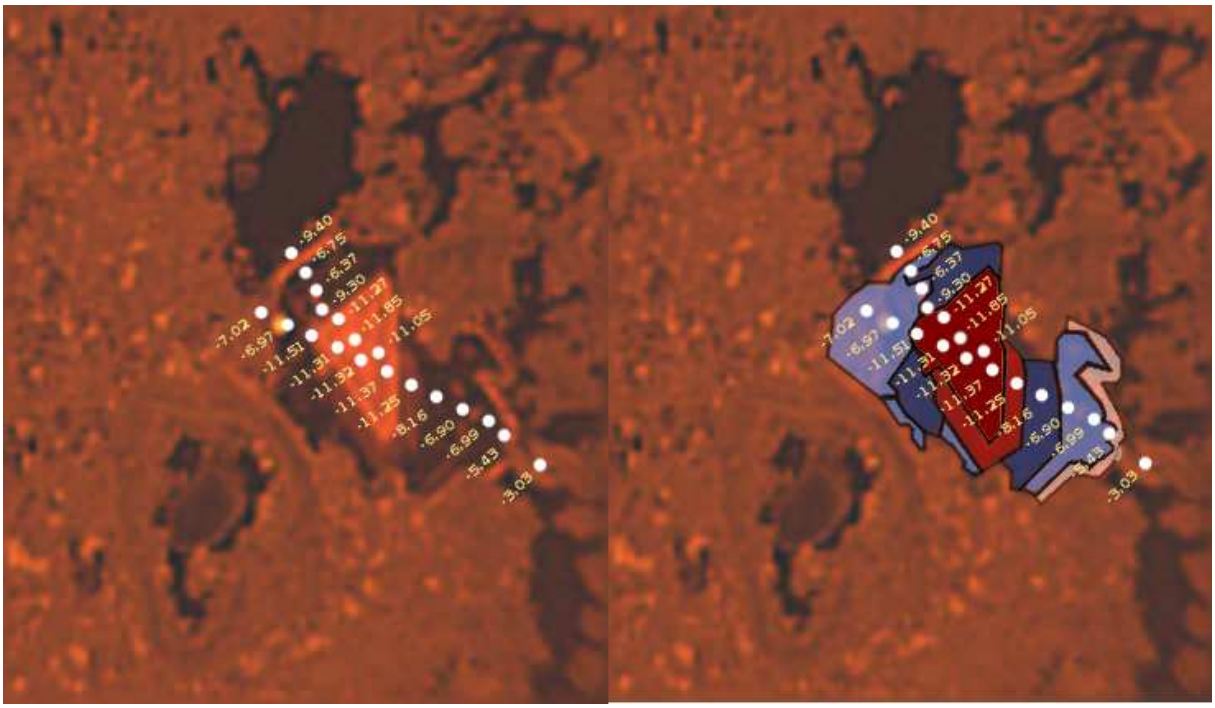

Figure 16. Cathodoluminescence photos of target 2 (oil leg) showing cement zonation (right) and oxygen isotope values decreasing away from the grain.

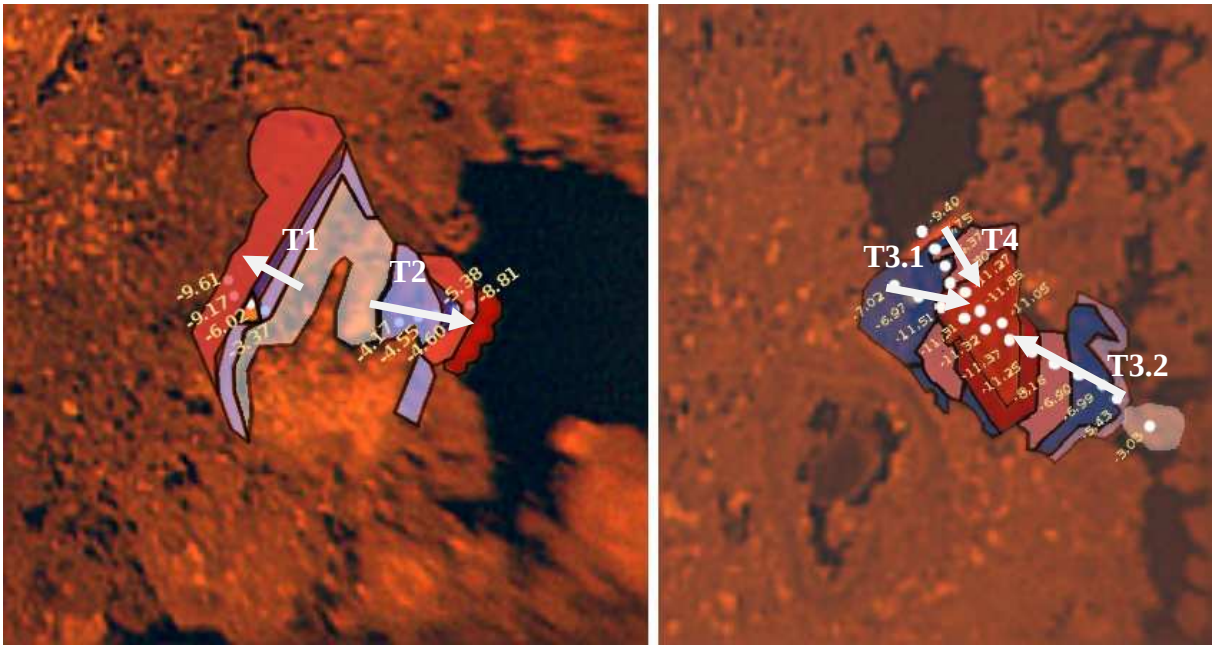

Figure 17. Syntaxial overgrowths with marked zones according to ion microprobe data. Growth directions shown by the arrows. Left: Target 1. Right: Target 2.

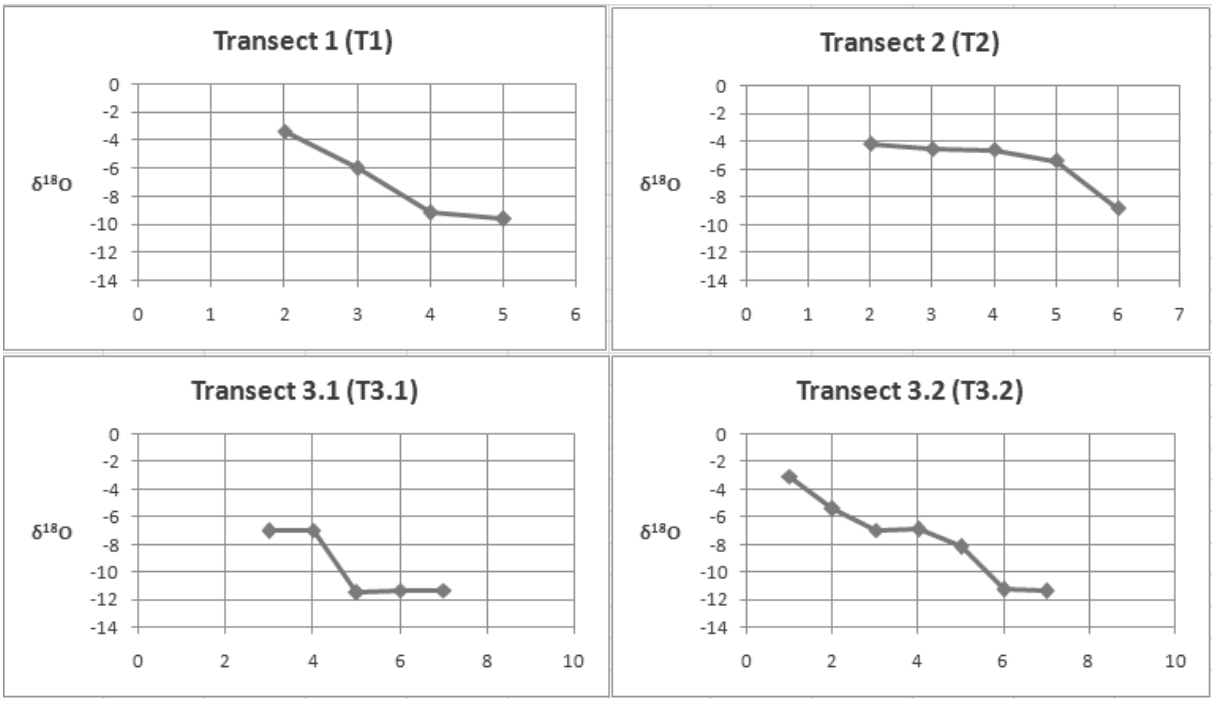

Figure 18. Transects along directions showed in Figure 17.

	Measured in Pixels									Percentage						
Target ID	Pore Area	Zone 1	Zone 2	Zone 3	Zone 4	Zone 5	Zone 6	Zone 7		Zone 1	Zone 2	Zone 3	Zone 4	Zone 5	Zone 6	Zone 7
1	1756	508	179	549	178					28.9	10.1	31.2	10.1	0	0	0
2	4330	2965	465	29						68.4	10.7	0.6	0	0	0	0
3	4474	1464	601	2241						32.7	13.4	50	0	0	0	0
4	4626	3355	697	214						72.5	15	4.6	0	0	0	0
5	4660	521	1109	881	2022					11.1	23.7	18.9	43.3	0	0	0
6	6292	3229	436	1869						51.3	6.9	29.7	0	0	0	0
7	6769	2157	933	3585						31.8	13.7	52.9	0	0	0	0
8	7347	4876	1249	537	215					66.3	17	7.3	2.9	0	0	0
9	8128	1494	2796	807						18.3	34.3	9.9	0	0	0	0
10	8471	3487	3096	584	271					41.1	36.5	6.8	3.1	0	0	0
11	12047	2803	4658	3526	883					23.2	38.6	29.2	7.3	0	0	0
12	13433	7513	3319	1373						55.9	24.7	10.2	0	0	0	0
13	14274	3546	2207	3123	4227					24.8	15.4	21.8	29.6	0	0	0
14	14993	7943	3138	1120						52.9	20.9	7.4	0	0	0	0
15	17058	7891	6842	274	2063					46.2	40.1	1.6	12	0	0	0
16	21426	7084	3326	4609	3747					33	15.5	21.5	17.4	0	0	0
17	24798	13150	6107	1212	1177					53	24.6	4.8	4.7	0	0	0
18	25209	2387	1516	3798	714	16749				9.4	6	15	2.8	66.4	0	0
19	29752	18495	3858	1427	1256	2324	439	182		62.1	12.9	4.7	4.2	7.8	1.4	0.6
20	37886	993	1842	11605	23427					2.6	4.8	30.6	61.8	0	0	0

Table 6. Syntaxial cement areas calculated from cathodoluminescence photos measured in pixels and shown in percentage of the pore space.

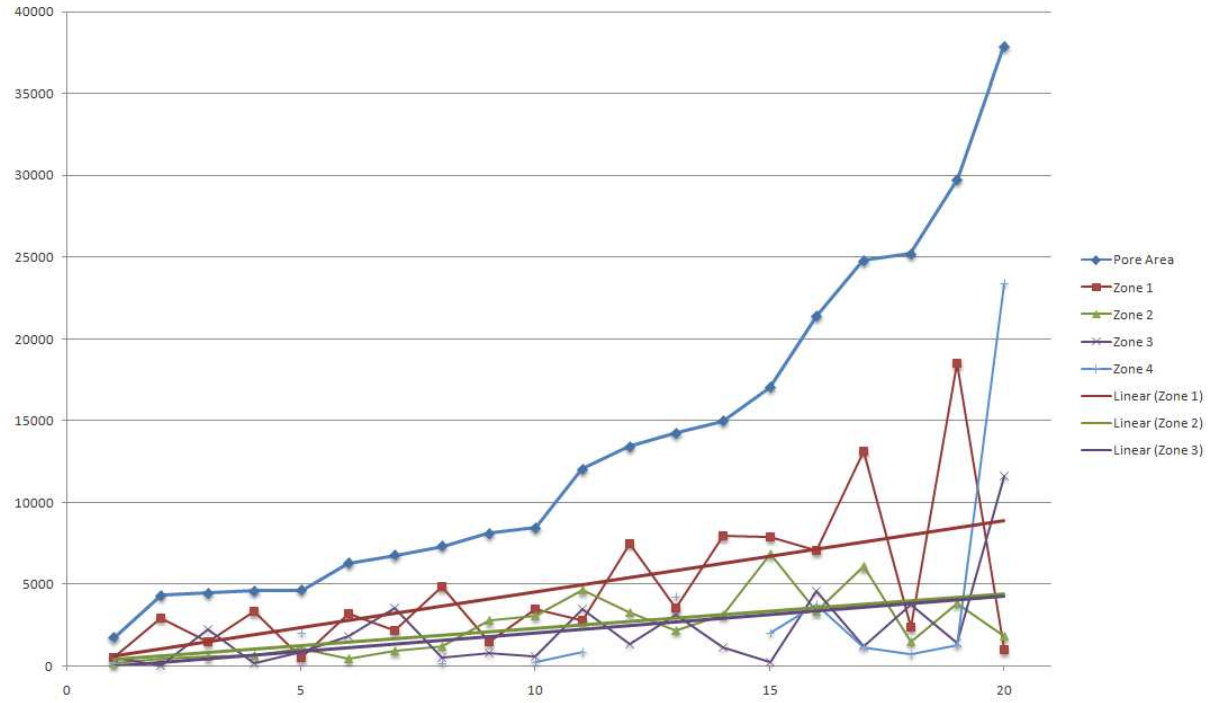

Figure 19. Cement zones area trends increasing with pore space (results from **Table 6**).

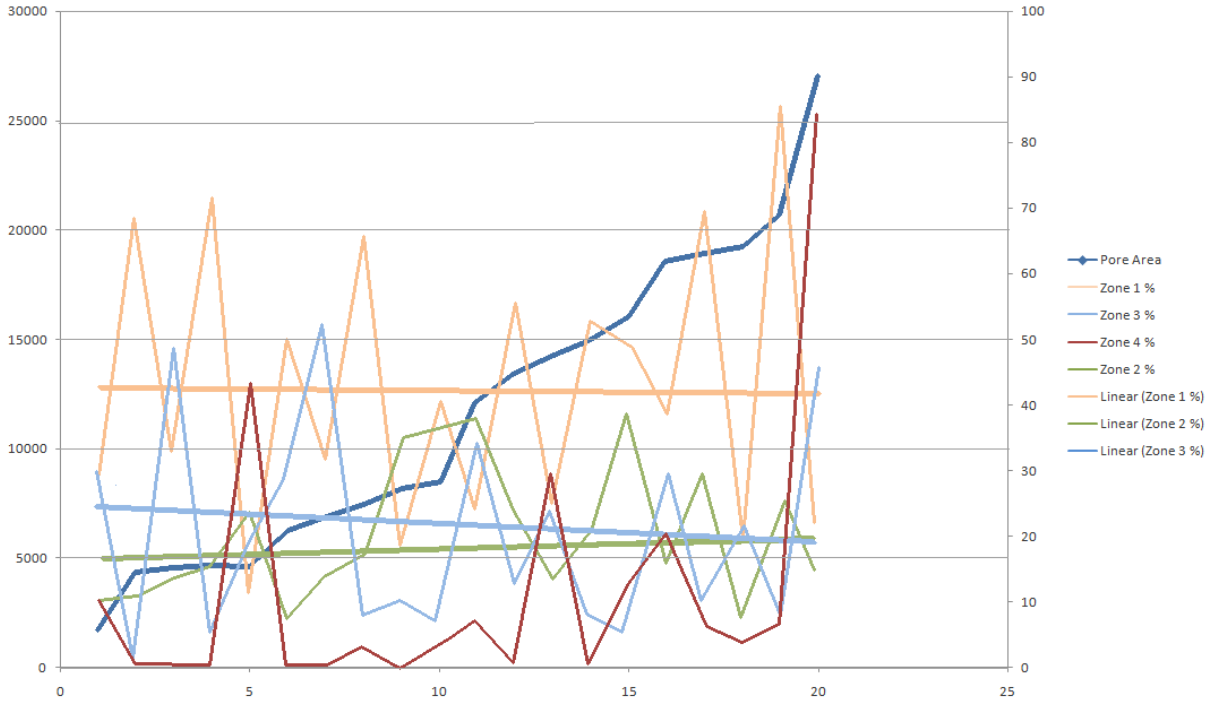

Figure 20. Cement zones percentage trends showing very little variation with pore space (results from **Table 6**).

Figure 21. Petrographic photos. **a)** Water leg sample. Syntaxial overgrowth (SO) growing of echinoderm fragment (Ech). Macroporosity (MAP) and microporosity (MIP). Foraminifera (F). **b)** Oil leg sample. Rim cement (RC) growing of peloids (P). Macroporosity (MAP). **c)** Oil lg sample. Foraminifera (F). Green Algae (GA), Intergranular porosity (IP). **d)** Water leg. Stylollyte (ST). **e)** Oil leg sample. Palorbitolina Lenticularis (PL).